JOURNAL OF GEOPHYSICAL RESEARCH, VOL. 95, NO. C10, PAGES 18,247–18,254, OCTOBER 15, 1990

On the Generation of Nonlinear Internal Kelvin Waves in a Rotating Channel

W. K. MELVILLE,[1] D. P. RENOUARD, AND X. ZHANG[2]

Institut de Mécanique de Grenoble, Saint-Martin d'Hères, France

Recent observations have shown that islands and constrictions may be the sites of significant internal wave activity in sea straits. In this paper we examine one generation mechanism: resonant forcing by transcritical flow past topography. Experiments were conducted on the large rotating platform at the Coriolis Laboratory, Institut de Mécanique de Grenoble, Grenoble, France. A slender body was towed through a two-layer stratified rotating channel, simulating the flow past an island or constriction in a strait. For a range of Froude numbers, blockage coefficients, and rotation rates, nonlinear internal Kelvin waves were generated upstream. The dependence of the wave parameters on the Froude number, Rossby number, and blockage coefficient was measured. The transition between subcritical and supercritical flow is found to occur at Froude numbers greater than unity, to depend on the blockage, but to be essentially independent of the internal Rossby radius of deformation. The results are compared with recent similar measurements of single-layer flows in nonrotating channels, and good agreement is obtained. The nonlinear Kelvin waves which are generated upstream are found to be similar in all respects to those described by Renouard et al. (1987).

1. INTRODUCTION

Satellite remote sensing and field experiments have shown that regions of abrupt topographic change can be the sites of significant internal wave activity in the coastal oceans. Examples of such topography include sills, islands, seamounts, and constrictions in straits. In the Strait of Gibraltar the exchange flow over bottom topography and past lateral constrictions gives rise to periodic generation of internal waves that propagate into the Alboran Sea [*Kinder*, 1984]. In the Gulf of California, tidal flows in the channels and past islands generate internal waves which are seen to propagate into the northern reaches of the gulf [*Fu and Holt*, 1982; *Maxworthy*, 1981]. If these waves were linear and dispersive, they would decay in amplitude due to dispersion and not be of significance far from the generation site. However, the possibility that a characteristic velocity of the flow, V, which generates the waves may be close to the velocity of the nth free mode of the system, c_n, makes resonance and finite amplitude effects of interest. The proximity to resonance is quantified by a Froude number, $F_n \equiv V/c_n$. If F_n is unity, the flow is said to be "critical"; if F_n is in the neighborhood of unity, then the flow is said to be "transcritical." In such flows the balance between nonlinearity and dispersion then permits the evolution of waves of (almost) permanent form which can propagate to large distances from the generation site.

There has been a great deal of interest in recent years in the resonant generation of nonlinear waves by moving disturbances in nonrotating systems (see *Wu* [1987] for a review), and some work on the forcing of nonlinear Rossby waves [*Patoine and Warn*, 1982; *Malanotte-Rizzoli*, 1984]; however, little has been done on the generation of nonlinear Kelvin waves by such a mechanism. Indeed, the subject of nonlinear Kelvin waves in a channel is one of some controversy. Experiments by *Maxworthy* [1983] and *Renouard et al.* [1987] show qualitative agreement in many respects but also display significant quantitative differences, for example, in the rate of decay of amplitude along the wave crest. Theoretical work [*Grimshaw*, 1985] casts serious doubt on whether weakly nonlinear Kelvin waves of permanent form exist for cases of weak rotation, that is, when the Rossby radius is much longer than the wavelength. This conclusion is consistent with the results of recent numerical work [*Katsis and Akylas*, 1987]. Most recently, *Melville et al.* [1989] and *Tomasson and Melville* [1990] have shown that Kelvin waves in a channel are unstable to direct and triad resonant interactions with Poincaré waves.

In this paper we wish to address the subject of the generation of nonlinear internal Kelvin waves by resonant forcing. In the nonrotating case it is now well known that a three-dimensional disturbance moving at transcritical speed can generate two-dimensional solitary waves upstream [see *Wu*, 1987; *Katsis and Akylas*, 1986]. The process by which the waves upstream evolve from three to two dimensions depends upon the nonlinear speed being a function of the wave amplitude. Reflection of the three-dimensional waves at the channel wall leads to an increase in amplitude and a corresponding increase in speed which ultimately produces a wave front normal to the wall [*Macomb*, 1986]. The process is akin to Mach reflection [*Miles*, 1977].

In a rotating channel this reflection process is clearly going to be influenced by rotation, and we anticipate that Kelvin waves may be generated upstream with the wave amplitude varying exponentially across the channel. In view of previous experimental and numerical results we anticipate that the wave crests may not be normal to the wall but curved, as first observed by *Maxworthy* [1983].

The experiments described below were designed to model the waves generated upstream by transcritical flow past an island or a constriction in a strait. They are of a preliminary nature and were undertaken to demonstrate the importance of rotation and topography in this class of flows.

[1]Permanently at R. M. Parsons Laboratory, Department of Civil Engineering, Massachusetts Institute of Technology, Cambridge.

[2]Permanently at Institute of Physical Oceanography, Shandong College of Oceanography, Qindao, People's Republic of China.

Paper number 90JC00487.
0148-0227/90/90JC-00487$05.00

2. EXPERIMENTS

The experiments were conducted on the 14-m rotating platform at the Coriolis Laboratory, Institut de Mécanique de Grenoble, France.

A steel-framed glass channel, 10 m long and 2 m wide, fitted with rails at the top of each longitudinal wall, was placed on the platform. The width of the working section could be set by positioning a movable wall parallel to one of the fixed walls of the channel so that the effective channel width could be varied between 50 cm and 2 m. For these experiments a channel width of 60 cm was chosen. A streamlined "ship-shaped" wooden body 60 cm long and 16 cm in diameter was suspended from a motorized carriage driven by a stabilized dc motor. The speed of the carriage was chosen by setting the motor controller and checked by timing the carriage over a section of the channel.

In a typical experiment the channel was spun up, and a lower saline layer of density ρ_2 was added to a depth of h_2. Subsequently, a layer of fresh water of density ρ_1 was slowly added (while the channel rotated) to give a total water depth of $(h_1 + h_2)$ with a typical interface thickness of less than 1 cm. The carriage was slowly moved to one end of the channel, and after all disturbances had decayed, the carriage was accelerated to a constant speed V in approximately 1–2 s and thereafter moved at this speed until it was stopped at 7 m down the channel. Displacement of the interface was measured by three electromechanical interface followers [*Renouard et al.*, 1987] fixed across the channel at 7.5 m and a fourth at 8.2 m on the right-hand wall to measure the wave speed by time delay relative to the followers at 7.5 m. An acoustic interface follower was attached to the carriage carrying the body at a position 16 cm ahead of the body. The combination of fixed and moving interface followers was dictated by the need to identify and measure the evolution of waves propagating upstream of the body.

Data were recorded on a digital computer and plotted for quality control after each run. Following one run, the body was slowly towed back down the channel. This procedure was repeated for a set of Froude numbers in the range of 0.59–1.3. After a set of runs at a fixed rotation rate (or Rossby radius) the platform would be very slowly accelerated or decelerated to a new (fixed) rotation rate, and the procedure repeated. This procedure was facilitated by a newly installed programmable speed control on the platform, which permits rotation periods in the range 18–999 s with a fractional error of less than 10^{-4}.

All of the experiments were run with a lower layer depth of 26 cm and upper layer depth of 4 cm. In all cases the normalized density change across the interface, $\delta\rho/\rho = (\rho_2 - \rho_1)/\rho_2$, was $O(10^{-2})$, and the platform rotation periods T_r were in the range 50–800 s.

Since the interface was thin in all experiments, the single (internal) Froude number F describing each experiment is given by

$$F = F_1 \equiv V/c_1$$

where

$$c_1^2 = g\frac{\delta\rho}{\rho}\frac{h_1h_2}{h_1 + h_2}$$

is the phase speed of the first internal mode. Surface wave effects were negligible, since the Froude number F_0 corresponding to the long surface wave speed c_0 was very much less than unity. The length scale imposed by rotation is the (internal) Rossby radius of deformation R, given by

$$R = c_1/f$$

where f is the Coriolis parameter.

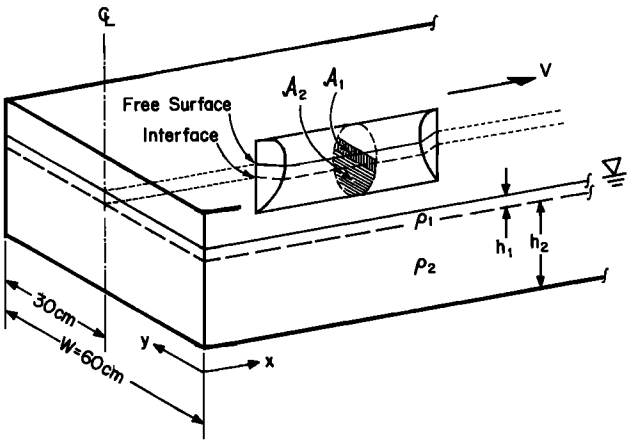

Fig. 1*a*. Schematic diagram of the channel and the towed body. Note that $\mathcal{A}_i$ is the maximum cross-sectional area of the body in the ith layer and $S_i = \mathcal{A}_i/(Wh_i)$ is the corresponding blockage coefficient.

The strength of the forcing due to the body is a function of the immersion and cross section of the body. Figure 1*a* shows a schematic of the channel and the body; Figure 1*b* shows the displaced volume v as a function of the depth of immersion, D. The results of similar experiments in nonrotating systems [*Ertekin et al.*, 1984] show that both the amplitude and frequency of generation of the waves upstream increase with the blockage coefficient, defined to be the fractional cross-sectional area of the channel blocked by the body. Experiments were run with D in the range [4, 13.5 cm], with most of the experiments run for D = 6.5 or 8 cm. Given the other constraints, these immersions were chosen to give a forcing sufficient to generate waves which could be resolved accurately in the length of the channel. In section 3 the experimental results will be presented with a parametric dependence on D. In section 4 it will be shown that they may be interpreted in terms of a modified blockage coefficient $\hat{S}$ (as derived by *Melville and Macomb* [1987]), which is a

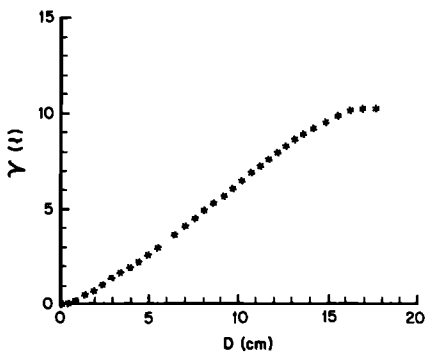

Fig. 1*b*. Immersed volume $\mathcal{V}$ of the moving body (in liters) as a function of the immersion D (in centimeters).

function of S_1 and S_2, the blockage coefficients for each layer.

3. RESULTS

Before undertaking a detailed analysis of the data it is worthwhile to show examples of the "raw" data. Figure 2 shows examples of the measurements with $(R, D) = [\infty, 6.5$ cm] and $F = 0.79$ (Figure 2*a*) and 0.95 (Figure 2*b*). Note that the upper trace corresponds to the interface measured relative to the body, and the lower three traces are from the fixed gauges. The time at which the body stops is marked and noted as T_s. In both cases we see that waves propagate upstream of the body while it is moving and separate earlier at the lower Froude number. The fixed gauges show that the leading waves are two-dimensional and aligned across the channel. The number of waves upstream decreases as the Froude number increases.

Figure 3 shows corresponding results with $R = 29$ cm and $(D, F) = (8$ cm, 0.71) in Figure 3*a* and $R = 28$ cm and $(D, F) = (6.5$ cm, 1.02) in Figure 3*b*. A number of features in these figures differ significantly from those in the nonrotating case. While waves separate from the body before it stops, they are no longer two-dimensional. First, there is a clear decrease in amplitude of the leading waves from the right-hand wall to the left-hand wall, qualitatively similar to a Kelvin wave. Second, the leading wave suffers a phase change across the channel similar to that observed in related experiments and numerical models of nonlinear Kelvin waves described in the introduction. Note also that the

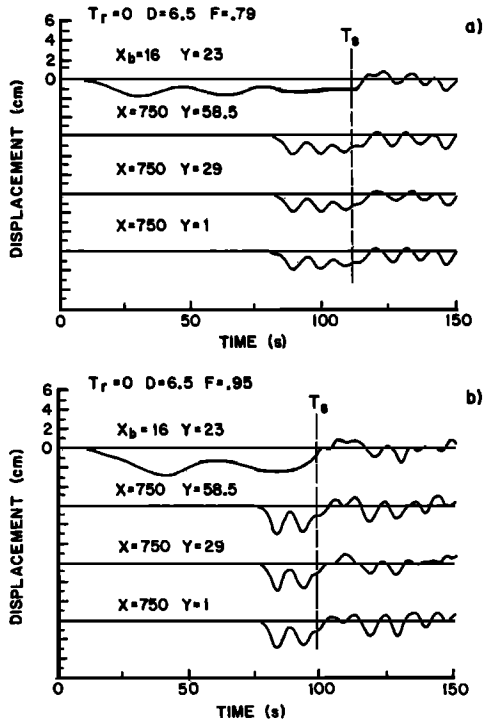

Fig. 2. Records of the interface height variation with time at 16 cm in front of the moving body (upper record in each figure) and at three fixed locations at $x = 750$ cm from the starting point of the body (which moved over 700 cm): at the right-hand wall ($y = 1$ cm), middle ($y = 29$ cm), and left-hand wall ($y = 58.5$ cm) of the channel. Here $\delta\rho/\rho = 0.0144$, $R = \infty$, $D = 6.5$ cm. T_s is the time at which the body stops. (*a*) $F = 0.79$. (*b*) $F = 0.95$.

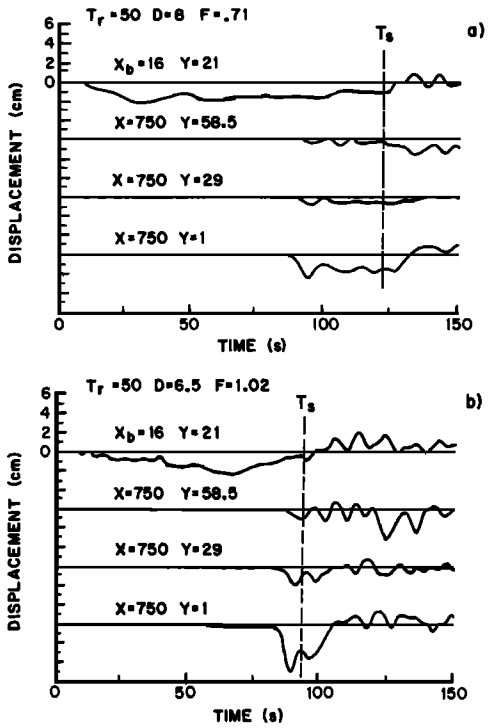

Fig. 3. Same as Figure 2, but with (*a*) $F = 0.71$, $\delta\rho/\rho = 0.0154$, $R = 29$ cm, $D = 8$ cm and (*b*) $F = 1.02$, $\delta\rho/\rho = 0.0140$, $R = 28$ cm, $D = 6.5$ cm.

leading waves are reflected at (or propagate around) the end of the channel and then have the largest amplitude on the left-hand wall (see especially Figure 3*a*). In view of the wave decay across the channel we may tentatively conclude that Kelvin waves are generated upstream. In view of the wave front curvature and previous experiments on unforced waves [*Maxworthy*, 1983; *Renouard et al.*, 1987] we may tentatively conclude that the waves upstream are nonlinear. The conclusion from these figures is that nonlinear Kelvin waves may be generated upstream of a moving disturbance. In the remainder of this section we shall expand upon this result with a detailed examination of the measurements.

Figure 4*a* shows the amplitude of the leading wave (at the center of the channel) as a function of the immersion depth for the nonrotating case. There is little dependence of the wave amplitude on the immersion depths at subcritical Froude numbers. At supercritical Froude numbers the wave amplitudes reach a maximum and decline for $D = 4$ and 13.5 cm, while they continue to increase for $D = 6.5$ and 8 cm. We shall discuss this behavior below. Figure 4*b* shows the amplitude of the leading wave (at the right-hand side of the channel) as a function of the Rossby radius for $D = 6.5$ cm. Within the scatter of the measurements we find a monotonic increase as the Rossby radius decreases. Corresponding results at the other immersion depths are qualitatively consistent with these data.

Figure 5*a* shows the amplitude of the first few waves for $D = 8$ cm and $R = \infty$. At subcritical Froude numbers there is a small decrease in amplitude with the second and subsequent waves. At supercritical Froude numbers the amplitude of the second wave decreases rapidly while that of the first continues to grow. The corresponding amplitudes for $D = 8$ cm and $R = 57$ cm are shown in Figure 5*b*, which is

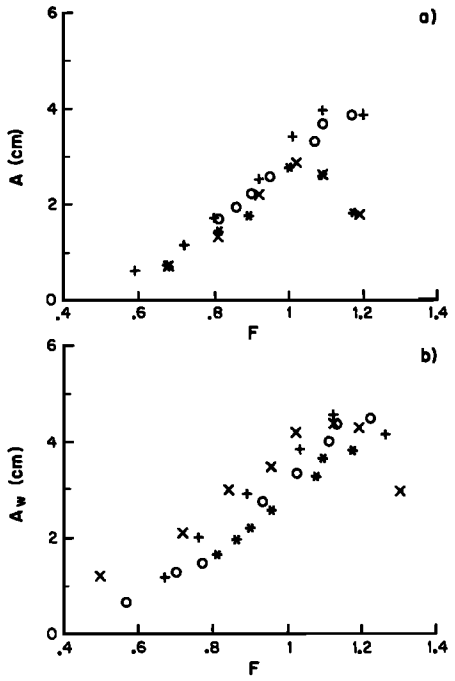

Fig. 4. (*a*) Amplitude A of the first wave recorded at $x = 750$ cm, $y = 29$ cm (middle of the channel), versus the Froude number for $R = \infty$: (asterisks) $\delta\rho/\rho = 0.0160$, $D = 4$ cm; (circles) $\delta\rho/\rho = 0.0144$, $D = 6.5$ cm; (plus signs) $\delta\rho/\rho = 0.0160$, $D = 8$ cm; and (crosses) $\delta\rho/\rho = 0.0160$, $D = 13.5$ cm. (*b*) Amplitude A_w of the first wave recorded at $x = 750$ cm, $y = 141$ cm (right-hand side of the channel), versus the Froude number: (asterisks) $\delta\rho/\rho = 0.0144$, $R = \infty$; (circles) $\delta\rho/\rho = 0.0117$, $R = 100.4$ cm; (plus signs) $\delta\rho/\rho = 0.0145$, $R = 56$ cm; and (crosses) $\delta\rho/\rho = 0.0140$, $R = 28$ cm, $D = 6.5$ cm.

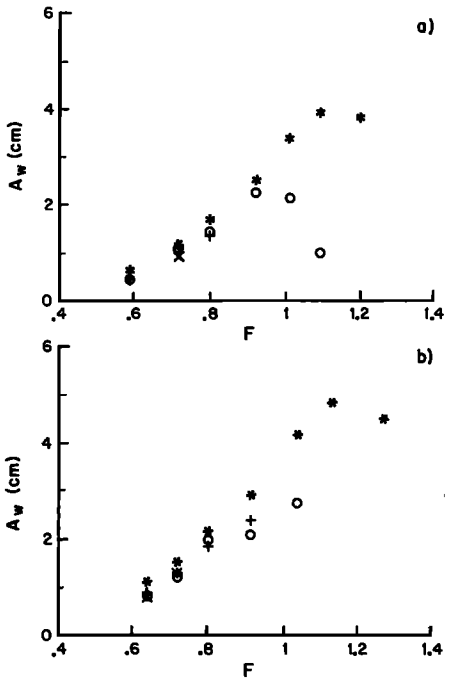

Fig. 5. Amplitude A_w of the first (asterisks), second (circles), third (plus signs), and fourth (crosses) waves recorded at $x = 750$ cm, $y = 1$ cm (right-hand side of the channel), as a function of the Froude number: (*a*) $\delta\rho/\rho = 0.0144$, $R = \infty$ and (*b*) $\delta\rho/\rho = 0.0154$, $R = 57$ cm, $D = 8$ cm.

qualitatively similar to Figure 5*a* with the exception that the second wave is still growing in amplitude at $F = 1$.

The time between the first and second waves (an estimate of the "period" of generation) for $R = \infty$ and D in the range [4, 13.5] cm is shown in Figure 6*a*. This period of wave generation decreases as the critical Froude number is approached from below. Corresponding results for $D = 8$ cm and R in the range [29 cm, ∞] (Figure 6*b*) show similar behavior (albeit with somewhat larger scatter) with little discernible dependence on R.

The essential nonlinearity of the waves upstream is shown in Figure 7 for both nonrotating and rotating experiments. The data show the increase in wave speed with amplitude corresponding to a two-layer Korteweg–de Vries (KdV) model:

$$\frac{c - c_1}{c_1} = \tfrac{1}{2} A_w \left[\frac{h_1 h_2}{h_2 - h_1}\right]^{-1}$$

where c is the speed and c_1 the corresponding linear speed. The effects of rotation are evident in the decay in amplitude along the crest of the leading wave across the channel, as shown in Figure 8 for $D = 8$ cm, R in the range [100, 29 cm], and $0.7 \leq F \leq 0.9$. The amplitudes along the crest are generally a little higher than

$$A(y)/A_w = \exp(-y/R)$$

This is consistent with earlier experiments on nonlinear waves in rotating channels [*Renouard et al.*, 1987]. Similar results to Figure 8 are found for $0.9 \leq F \leq 1.3$. As seen earlier in Figure 3, the leading waves in the rotating system are not normal to the sidewalls of the channel but suffer a phase shift across the channel. The role of rotation in leading to a phase shift of the leading wave across the channel is demonstrated in Figures 9*a* and 9*b*, which show the phase shift for $D = 6.5$ cm and $R = [\infty, 28$ cm], respectively, and a range of Froude numbers. This effect is quantified in Figure

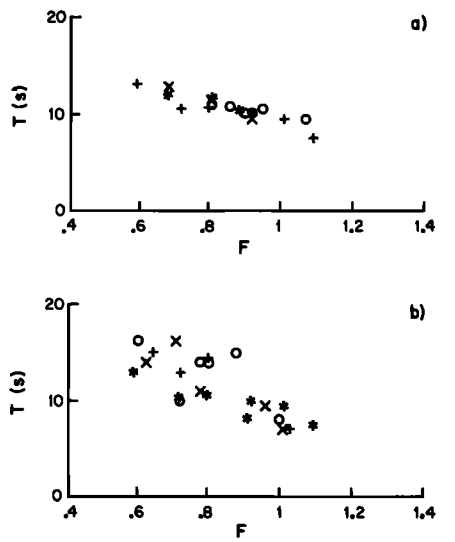

Fig. 6. Time between the first and the second wave recorded at a fixed location, as a function of the Froude number: (*a*) (asterisks) $\delta\rho/\rho = 0.0160$, $D = 4$ cm; (circles) $\delta\rho/\rho = 0.0144$, $D = 6.5$ cm; (plus signs) $\delta\rho/\rho = 0.0160$, $D = 8$ cm; and (crosses) $\delta\rho/\rho = 0.0160$, $D = 13.5$ cm, $R = \infty$; and (*b*) (asterisks) $\delta\rho/\rho = 0.0160$, $R = \infty$; (circles) $\delta\rho/\rho = 0.0117$, $R = 100.4$ cm; (plus signs) $\delta\rho/\rho = 0.0154$, $R = 56$ cm; and (crosses) $\delta\rho/\rho = 0/0154$, $R = 28$ cm, $D = 8$ cm.

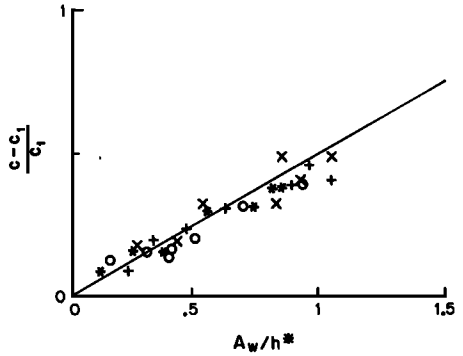

Fig. 7. Increase in wave speed with amplitude for both rotating (circles, plus signs, crosses) and nonrotating (asterisks) experiments. The solid line corresponds to $(c - c_1)/c_1 = \frac{1}{2} A_w/H^*$ with $H^* = h_1h_2/(h_2 - h_1)$.

9c, where the dimensionless phase shift of the crest is plotted as a function of the distance across the channel. In this figure the dimensionless scaling due to *Zhang* [1986] appears to collapse the data for $D = 6.5$ and 8 cm, $0.7 \leq F \leq 0.9$. Corresponding data for $0.9 \leq F \leq 1.3$ show much larger scatter. The scatter in the results at the larger Froude numbers is perhaps due to the fact that the leading wave had insufficient time to develop before reaching the fixed interface followers (see also Figures 9a and 9b). The time at which the leading wave reached a maximum at the moving interface follower (taken to be the "separation time"), and the time of the first maximum at the fixed interface follower in the center of the channel, gave an elapsed time which could be transformed to a distance X_s using the nonlinear wave speed. This is an estimate of the distance traveled by the wave after separating from the body. This distance is plotted versus Froude number in Figure 10a for $R = \infty$ and shows that for small Froude numbers, X_s is sensibly independent of the depth of immersion. At larger Froude numbers a dependence on D is evident and will be discussed in section 4. In Figure 10b, X_s is plotted for all D and R. Comparison with Figure 10a shows that there is no discernible dependence on R for the range of parameters used in these experiments.

Finally, we consider the leading wave profile. In all cases the forward face of the wave was well described by a sech^2

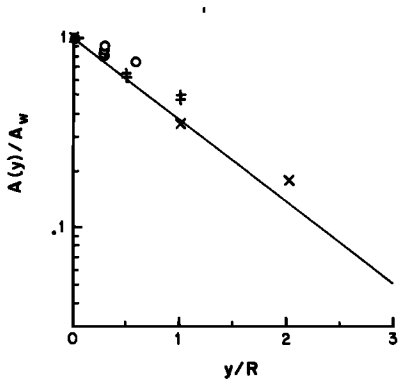

Fig. 8. Decay in amplitude along the crest of the leading wave across the channel, for $D = 8$ cm, $0.7 \leq F \leq 0.9$: (circles) $\delta\rho/\rho = 0$ and 0.0117, $R = 100.4$ cm; (plus signs) $\delta\rho/\rho = 0.0154$, $R = 56$ cm; and (crosses) $\delta\rho/\rho = 0.0154$, $R = 28$ cm.

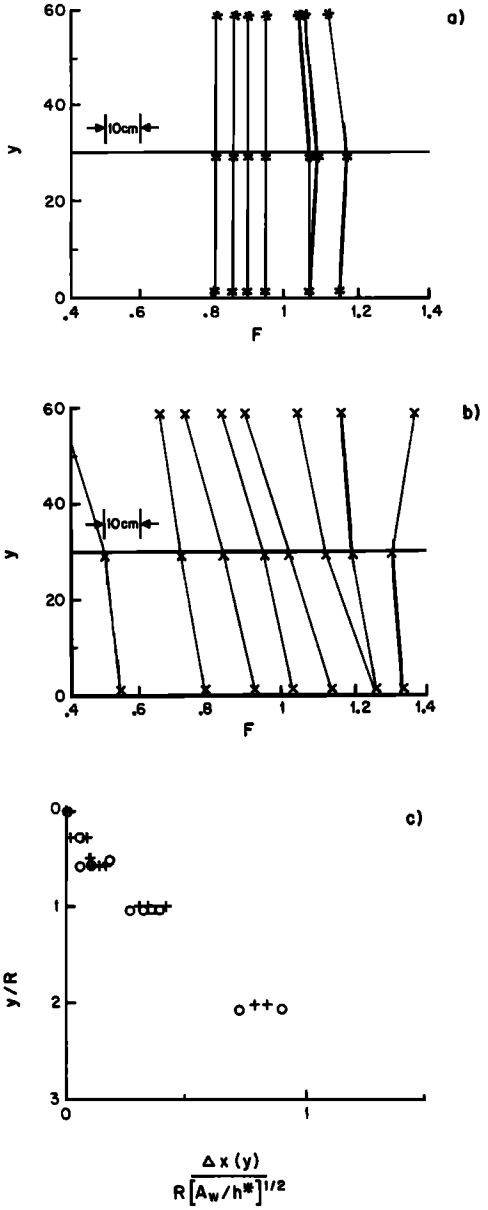

Fig. 9. (*a*) Plan view of the crest of the leading waves for various Froude numbers. The lower scale and lowest symbol for each experiment indicates the Froude number value, while the upper scale (middle of figure) shows the spatial phase shift across the channel. Here $\delta\rho/\rho = 0.0144$, $D = 6.5$ cm, $R = \infty$. (*b*) Here $\delta\rho/\rho = 0.0140$, $D = 6.5$ cm, $R = 28$ cm. (*c*) Nondimensional spatial phase shift across the channel for various radii of deformation, and $0.7 \leq F \leq 0.9$: (circles) $D = 6.5$ cm and (plus signs) $D = 9$ cm.

profile (see, for example, Figure 11). However, the KdV amplitude-wavelength relationship is not satisfied exactly: the wavelength is approximately proportional to the square root of the amplitude, but the proportionality constant is larger than the two-layer KdV model result (Figure 12) [cf. *Renouard et al.*, 1987].

4. Discussion

The results presented above clearly show that nonlinear internal Kelvin waves may be generated upstream by flows past a constriction or island in a rotating channel. There are, as far as we are aware, no theoretical or numerical predic-

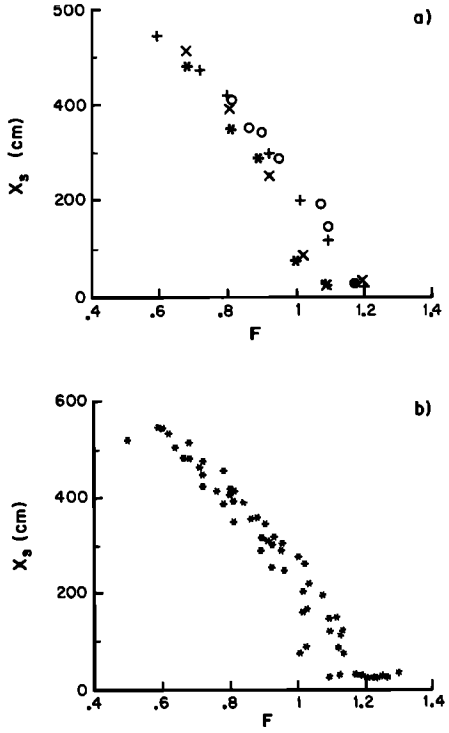

Fig. 10. Estimated distance X_s traveled by the first wave after it separates from the moving body, as a function of the Froude number: (*a*) $R = \infty$: D = (asterisks) 4 cm, (circles) 6.5 cm, (plus signs) 8 cm, and (crosses) 13.5 cm. (*b*) All experiments for all R and D.

tions of such flows with which we may compare our results. However, some comparisons with the results of single-layer nonrotating flows are possible and confirm the quality of the data presented here. Furthermore, some physical interpretation of the data is justified and will be presented.

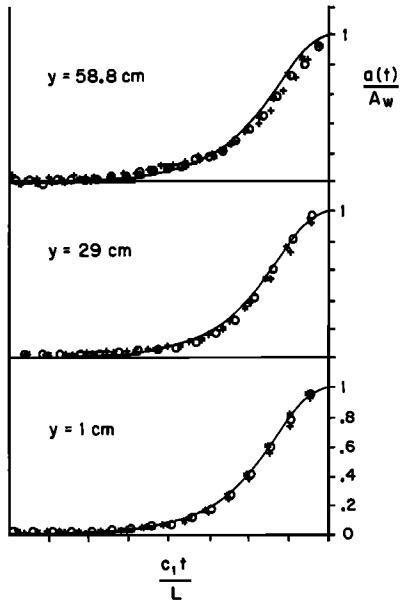

Fig. 11. Nondimensional shape of the forward face of the leading wave at the three stations across the channel, for $\delta\rho/\rho = 0.0154$, $R = 57$ cm, $D = 8$ cm, and (asterisks) $F = 0.64$, (circles) $F = 1.03$, and (plus signs) $F = 1.26$. Solid line corresponds to sech^2 profile. Note that the length scale L is given by $L^2 = \frac{4}{3}h_1^2h_2^2/[A_w(h_2 - h_1)]$.

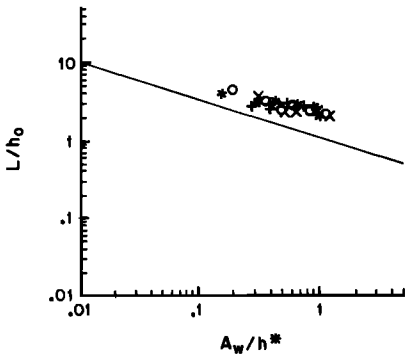

Fig. 12. Relation between nondimensional wavelength, $L/(\frac{4}{3}h_1h_2)^{1/2}$ amplitude, $A_w/[h_1h_2/(h_2 - h_1)]$, for all experiments with rotation, and $D = 8$ cm. The solid line corresponds to the KdV relation, with a $(-1/2)$ slope.

In a recent paper, *Melville and Macomb* [1987] showed that the theoretical formulation of a two-layer flow past a constriction in a strait could be transformed into an equivalent single-layer problem with a transformation of variables and boundary conditions. In the single-layer case the blockage coefficient is just the fractional area of the channel occupied by the constriction. In the two-layer case the internal mode is not excited by a body having a shape uniform with depth through the two layers.

It is the representation of the geometry of the body in terms of the internal (displacement) modes of the wave field which leads to forcing of internal waves. Thus in order to force a first mode internal wave the width of the body must vary with depth so that the effective body geometry over the water column has a nonzero mode corresponding to the first mode internal wave. For the two-layer case the equivalent blockage coefficient becomes

$$S = \frac{|h_2 - h_1|}{h_1 + h_2}|S_2 - S_1|$$

where h_1 and h_2 are the upper and lower layer depths, respectively, and S_1 and S_2 are the corresponding blockage coefficients for each layer. That is, S_i is the fraction of the cross section of the ith layer blocked by the body. Applying this result to our experiments, we find that the equivalent blockage coefficients are as shown in Table 1.

Referring to Figure 4*a* ($R = \infty$),we see that for fixed F there is, within the scatter of the results, an increase in the amplitude of the waves generated upstream with increasing S. This is consistent with the available numerical and experimental evidence for the equivalent single-layer case [cf. *Ertekin et al.*, 1984; *Katsis and Akylas*, 1986; *Macomb*, 1986] at subcritical Froude numbers. To demonstrate this, in

TABLE 1. Depth of the Immersion D of the Body and Equivalent Blockage Coefficients S for the Two-layer System

D, cm	S
4	0.10
6.5	0.13
8	0.14
13.5	0.09

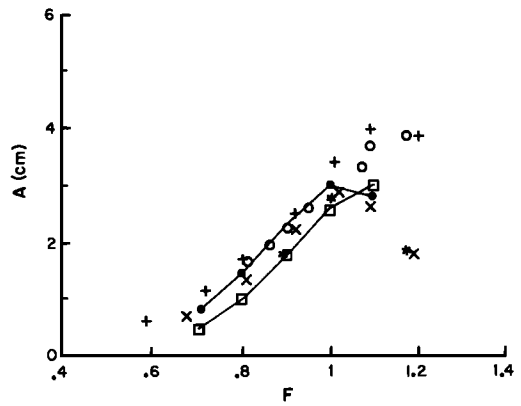

Fig. 13. Same as Figure 4*a* with measurements of *Ertekin et al.* [1984, Figure 10] rescaled according to *Melville and Macomb* [1987] for $S = 0.09$ (curve with squares) and $S = 0.14$ (curve with solid circles).

Figure 13 we have replotted Figure 4*a* along with the experimental data of *Ertekin et al.* [1984] for $S = 0.09$ and 0.14, the range of blockage coefficients in our experiments. The data of *Ertekin et al.* [1984] have been rescaled according to the transformation of *Melville and Macomb* [1987] in which the displacement is scaled with the quiescent depth for the single-layer case and $h_1h_2/(h_1 - h_2)$ for the two-layer case. We see that our amplitudes are a little below those of Ertekin et al., but given the scatter in both sets of experiments we consider the agreement to be good, especially below $F = 1$. Above $F = 1$ the data diverge for the higher blockage coefficients with the amplitude of the single-layer waves being limited by breaking.

Ertekin et al. [1984] also measured the period of generation of waves upstream and presented the data as a dimensionless time $T^* = VT/h$, where V is the speed of the body, T is the period in the frame moving with the body, and h is the undisturbed depth. Using the results of *Melville and Macomb* [1987], the equivalent dimensionless time for the two-layer case is

$$T^* = \left(\frac{g\,\delta\rho/\rho}{h}\right)^{1/2} T$$

where g is the gravitational acceleration, $\delta\rho/\rho$ is the fractional change in density across the interface, and h is the total depth of the two layers. From Figure 2 we find that $T^* = 23$ (Figure 2*a*) and 28 (Figure 2*b*). The corresponding values from the measurements of *Ertekin et al.* [1984] for $F = 0.8$ and 1 are 23 and 29, respectively. On the basis of the above results we conclude that the two-layer experiments in the absence of rotation agree well with the available single-layer experiments when compared according to the transformation of *Melville and Macomb* [1987].

Figure 4*a* also shows that for fixed S the amplitude of the leading wave increases with F to a maximum which is dependent on the equivalent blockage coefficient, the maximum increasing as S increases. For the smaller S the maximum amplitude corresponds to the Froude number at which there is a transition from unsteady flow upstream to steady supercritical flow in the neighborhood of the body, that is, the Froude number F_c at which the leading wave begins to travel at the same speed as the body. Figure 10*a* shows that for the smaller values of S, waves do not travel upstream relative to the body for $F > F_c$. For the larger values of S it appears that F_c may be equal to the largest Froude numbers tested; however, at these Froude numbers there is some uncertainty, since the waves may not have been fully developed before the body stopped. Notwithstanding this uncertainty, the transition clearly occurs at higher Froude numbers and wave amplitudes for the larger blockage coefficients. Thus the transition to supercritical flow occurs at Froude numbers greater than unity and is dependent on the blockage coefficient. This contrasts with the classical use of $F = 1$ as the boundary between subcritical and supercritical flow.

From Figure 4*b* it can be seen that for a given blockage coefficient the wave amplitude (at the right-hand wall) increases as F increases and R decreases, reaching a maximum at a value of F_c which appears to be independent of R. The smallest Rossby radius considered was approximately 50% of the channel width and led to increases of wave amplitude of approximately 20% ($F = 1.15$) to 100% ($F = 0.6$). These results emphasize the importance of accounting for rotation in the flow in straits when the internal Rossby radius of deformation is comparable to or less than the width of the strait. For example, in the Strait of Gibraltar the internal Rossby radius of deformation may be $O(10$ km), comparable to the width of the strait.

It is also significant that the time scale for generation of the waves upstream may be short compared to the major tidal cycles. For example, for dimensionless blockage coefficients comparable to those employed here the period of wave generation may be $O(1$ hour) for typical stratifications and depths of the coastal oceans (i.e., $\delta\rho/\rho \sim O(10^{-3})$, $h \sim O(10^2)$ m). Thus care should be exercised in considering the time scales over which quasi-steady models of flows through straits are valid.

Finally, we wish to emphasize the important difference introduced by rotation. Without rotation, through a process of nonlinear reflection at the sidewalls (as described by *Macomb* [1986]) the initially three-dimensional disturbance ahead of the body evolves into two-dimensional waves spanning the channel. This is clearly shown in Figure 9*a*, where at the subcritical Froude numbers there is no discernible phase change across the channel. We believe that the small changes in the phase at the higher Froude numbers in this figure may be due to the fact that the waves may not have completely evolved in the available channel length (see also Figure 9*b*). Another explanation suggested by the shape for the highest Froude number is that the leading wave is a steady bow wake shed by the body after stopping. This would be consistent with our earlier discussion of the leading wave in the neighborhood of the maximum amplitude, which is based in part on the results in Figure 10. When rotation is introduced, the waves upstream remain three-dimensional and evolve very much like the nonlinear interfacial waves observed by *Renouard et al.* [1987], exhibiting curved fronts (compare Figures 8 and 9*c*) and profiles comparable to Boussinesq solitary waves (compare Figures 11 and 12).

Acknowledgments. The authors wish to thank G. Chabert d'Hieres for many fruitful discussions, and H. Didelle, R. Carcel, and C. Roche for assistance in designing and conducting the experiments. One of us (W.K.M.) wishes to thank M. Piau and G. Chabert d'Hieres for their generous hospitality during the course of

the work; and the CNRS, The University of Grenoble, and the John Simon Guggenheim Memorial Foundation for their support. This research is supported by the Office of Naval Research (Coastal Studies).

REFERENCES

Ertekin, R. C., W. C. Webster, and J. V. Wehausen, Ship generated solitons, in *15th Symposium on Naval Hydrodynamics*, pp. 1–15, National Academy of Sciences, Washington, D. C., 1984.

Fu, L. L., and B. Holt, Seasat views oceans and sea ice with synthetic aperture radar, *JPL Publ. 81-120, 1982.*

Grimshaw, R., Evolution equations for weakly nonlinear, long internal waves in a rotating fluid, *Stud. Appl. Math., 73*, 1–100, 1985.

Katsis, C., and T. R. Akylas, On the excitation of long nonlinear water waves by a moving pressure distribution, 2, Three-dimensional effects, *J. Fluid Mech., 177*, 49–65, 1986.

Katsis, C., and T. R. Akylas, Solitary internal waves in a rotating channel: A numerical study, *Phys. Fluids, 30*, 297–301, 1987.

Kinder, T. H., Net mass transport by internal waves near the Strait of Gibraltar, *Geophys. Res. Lett., 11*, 987–990, 1984.

Macomb, E. S., The interaction of nonlinear waves and currents with coastal topography, M.S. thesis, Mass. Inst. of Technol., Cambridge, 1986.

Malanotte-Rizzoli, P., Boundary-forced planetary radiation, *J. Phys. Oceanogr., 14*, 1032–1046, 1984.

Maxworthy, T., Nonlinear dispersive waves in the laboratory and nature, in *Nonlinear Properties of Internal Waves*, edited by B. West, pp. 11–46, American Institute of Physics, New York, 1981.

Maxworthy, T., Experiments on solitary internal Kelvin waves, *J. Fluid Mech., 129*, 365–383, 1983.

Melville, W. K., and E. Macomb, Transcritical stratified flow in straits, in *Stratified Flows*, edited by E. J. List and G. H. Jirka, D. Reidel, Hingham, Mass., 1987.

Miles, J. W., Resonantly interacting solitary waves, *J. Fluid Mech., 79*, 171–179, 1977.

Patoine, A., and T. Warn, The interaction of long, quasi-steady baroclinic waves with topography, *J. Atmos. Sci., 39*, 1018–1025, 1982.

Renouard, D. P., G. Chabert D'Hieres, and X. Zhang, An experimental study of strongly nonlinear waves in a rotating system, *J. Fluid Mech., 177*, 381–394, 1987.

Tomasson, G. G., and W. K. Melville, Nonlinear and dispersive effects in Kelvin waves, *Phys. Fluids A, 2*, 189–193, 1990.

Wu, T. Y.-T., Generation of upstream advancing solitons by moving disturbances, *J. Fluid Mech., 184*, 75–99, 1987.

Zhang, X., Contribution à l'étude des ondes internes non-linéaires en présence d'une topographie ou de rotation, thèse de doctorat, Inst. de Méc. de Grenoble, Saint-Martin d'Hères, France, 1986.

W. K. Melville, R. M. Parsons Laboratory, Department of Civil Engineering, Massachusetts Institute of Technology, Cambridge, MA 02139.

D. P. Renouard, Institut de Mécanique de Grenoble, B. P. 68, 38402 Saint-Martin d'Hères, France.

X. Zhang, Institute of Physical Oceanography, Shandong College of Oceanography, P. O. Box 90, Qindao, People's Republic of China.

(Received August 1, 1989;
accepted August 8, 1989.)